The Role of Zonal Flows and Predator-Prey Oscillations in the L-H and H-L transition

L. Schmitz[1], L. Zeng[1], T.L. Rhodes[1], J.C. Hillesheim[1], G.R. McKee[2], Z. Yan[2], W.A. Peebles[1], R.J. Groebner[3], K.H. Burrell[3], G.R. Tynan[4], E.J. Doyle[1] and G. Wang[1]

[1]*University of California, Los Angeles, Los Angeles, California 90095-7799, USA*
[2]*University of Wisconsin-Madison, Madison, WI 53706, USA*
[3]*General Atomics, San Diego, California CA 92186-5608, USA*
[4]*University of California, San Diego, La Jolla, CA 92093-0417, USA*

Understanding the trigger dynamics and power threshold of the L-H transition is important for extrapolating present tokamak performance to burning plasma regimes. Zonal Flow (ZF) generation via the Reynolds stress due to drift wave turbulence has been proposed as trigger of the L-H transition. We present direct experimental evidence of low frequency ZFs in the form of limit cycle oscillations (LCO), initiating turbulence reduction preceding the L-H transition, near the power threshold, in so-called "dithering" H-mode transitions in low to medium density plasmas ($1.8\text{x}10^{19}$ m^{-3} $\leq \langle n \rangle \leq$ $3.5\text{x}10^{19}$ m^{-3}) [1]. Earlier evidence potentially consistent with the interaction of turbulence and time-dependent ZF flows has also been reported from a number of experiments [2–6]. Here we examine the detailed spatio-temporal evolution of the **E×B** shear layer and turbulence characteristics including the radial correlation of turbulence and **E×B** flow. Figure 1(a) shows a contour plot of the **E×B** velocity at and inside the last closed flux surface (LCFS), determined from turbulence poloidal advection via multichannel microwave Doppler Backscattering (DBS) [7,8], which probes simultaneously 12 radial locations using co-linear launch/receive optics. When the LCO starts at 1271.7 ms, the **E×B** velocity periodically becomes negative at and just inside the last closed flux surface (LCFS). The negative flow increases with time and the flow layer expands radially. Around 1288 ms, the transition to ELM-free H-mode takes place after a final transient, characterized by a wider, steady flow layer. Figure 1(b) shows that the normalized

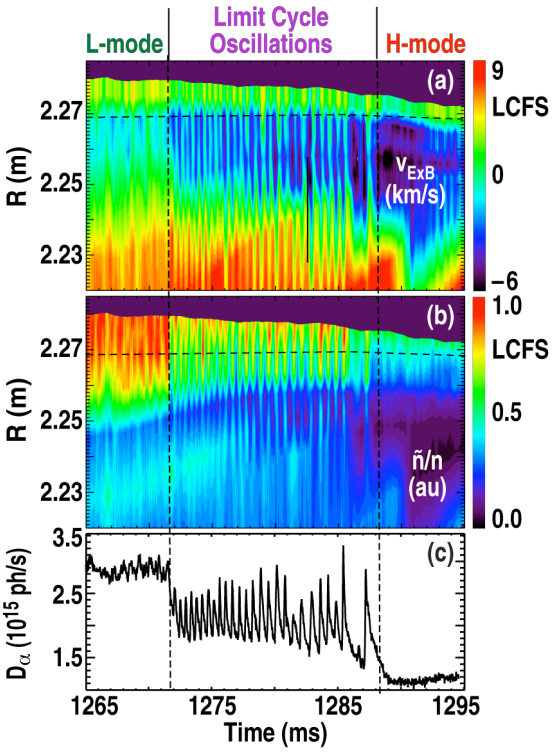

Fig. 1. (a) **E×B** velocity; (b) rms normalized density fluctuation level ñ/n; (c) D_α divertor recycling light during the transition from L-mode through the LCO phase to H-mode.

density fluctuation level ñ/n (proportional to the amplitude of the scattered DBS signal) is periodically reduced during the LCO (the probed poloidal wavenumber is $k_\theta\rho_s$~0.45 with $\Delta k_\theta/k_\theta$~0.3, encompassing the most unstable Ion Temperature Gradient (ITG) and Resistive Ballooning Mode wavenumber range). Sustained turbulence reduction is observed at the final H-mode transition [Fig. 1(b)]. We have shown in [1] that the LCO has all the characteristics of a Zonal Flow predator-prey oscillation [9], characterized by toroidal/poloidal symmetry of the flow (n=0, m=0), with a finite radial wavenumber (k_r~0.7 cm^{-1} at t=1275 ms) of the flow, and a 90º phase lag of the ZF with respect to the density fluctuation level ñ/n.

Strong evidence for turbulence suppression by Zonal Flow shear is provided by a comparison of the **E×B** shearing rate at the LCFS (calculated as the difference of the probed **E×B** velocities between two DBS probing locations, divided by the radial distance) and the turbulence decorrelation rate (calculated from the auto-correlation time of the density fluctuation level as determined by DBS). In the presence of **E×B** advection, the lab frame turbulence decorrelation rate is given by $\Delta\omega_D^{lab}=\Delta\omega_D(v_{\mathbf{E\times B}}/\lambda_\theta)[\Delta\omega_D^{-2}+\lambda_\theta^2/v_{\mathbf{E\times B}}^2]^{1/2}$. Taking the poloidal correlation length as $\lambda_\theta > 4\lambda_r$ (in agreement with experimental results, as explained below) and using the measured L-mode decorrelation rate in the absence of advection, we find $\Delta\omega_D^{-1} < l_\theta/v_{\mathbf{E\times B}}$, and to good approximation $\Delta\omega_D^{lab} \sim\Delta\omega_D$. Figure 2 shows that turbulence reduction coincides with times when the shearing rate (measured across the LCFS) exceeds the decorrelation rate. Initial suppression appears to be triggered by a reduction in the decorrelation rate relative to the **E×B** shearing rate. As the relative errors of both quantities are substantial (±28% for the shearing rate and ±11–16% for the decorrelation rate) the result has been confirmed via phase-lock analysis with respect to the LCO.

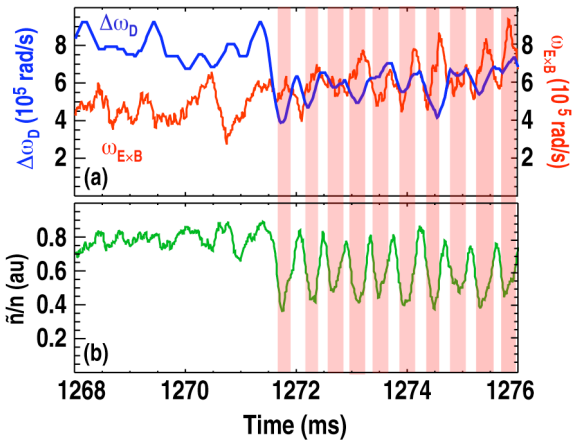

Fig. 2. (a) Turbulence decorrelation rate $\Delta\omega_D$ and **E×B** shearing rate $\omega_{\mathbf{E\times B}}$ during the transition from L-mode to LCO; (b) normalized rms density fluctuation level from DBS.

The radial turbulence correlation length λ_r has been determined from five DBS channels probing a radial range of ≈1 cm (with a channel spacing $\Delta r \approx 0.25$ cm). During time periods when the turbulence level is reduced in the LCO, the correlation length is also reduced by about 30%, as shown in Fig. 3(a,b). During the final H-mode transition, λ_r is further reduced by 40% compared to the LCO time periods with turbulence reduction. The DBS diagnostic cannot presently provide a measurement of poloidal turbulence correlation length. However,

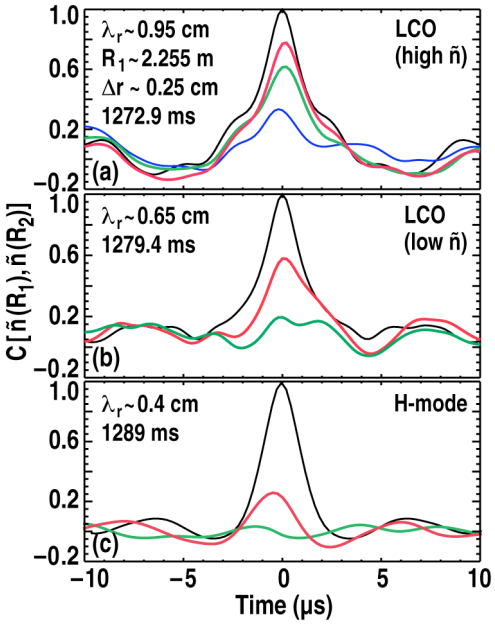

Fig. 3. Auto-correlation and radial cross-correlation coefficients between a reference channel and 2–3 radially displaced probing radii, and derived radial correlation length of density fluctuations during the LCO (a,b) and during ELM-free H-mode (c).

highly anisotropic eddies with $l_\theta \gg l_r$ have been observed via Beam Emission Spectroscopy (BES, sensitive to $k_\theta \leq 3$ cm^{-1}) with l_θ increasing from 5 cm in L-mode to 7 cm in H-mode. Both the observed reduction in radial correlation length and the increasing anisotropy and increasing poloidal correlation length support the physical picture of shear stabilization [10,11], via ZF shear in the LCO during the reduced-ñ time periods and, and via equilibrium **E×B** shear in H-mode.

The limit cycle between ñ/n and $v_{\mathbf{E\times B}}$ is shown in Fig. 4(a) (green symbols correspond to L-mode; red symbols to H-mode; purple/magenta symbols (1 cm and 2.5 cm inside LCFS) represent the LCO (measured at 1278±1.5 ms). The front of the ZF is observed to propagate radially inward from the LCFS, initially with a velocity $v_r \sim \Delta R/\Delta\tau \sim 120$ m/s, as deduced from the radial cross correlation of the turbulence amplitude [Fig. 4(b)]. This observation may indicate that the ZF is driven near the LCFS where fluctuation levels are highest. Just before the H-mode transition (t=1285 ms), the radial phase velocity increases to ~410 m/s near the time of the final H-mode transition [Fig. 4(c)]. Phase fronts are therefore more aligned radially at the later time, while the LCO frequency decreases. The transition to ELM-free H-mode (characterized by sustained turbulence/transport reduction) is likely secured by the increase in equilibrium flow shear due to the increasing ion pressure gradient after the initial turbulence reduction, as discussed in detail in [1]. The reduced radial propagation delay of the **E×B** flow as shown in Fig. 4(c)] coincides with increasing influence of the equilibrium electric field shear (as discussed in [1]) and may indicate a reduced relative influence of the Reynolds stress radial gradient [12,5] in flow generation near the

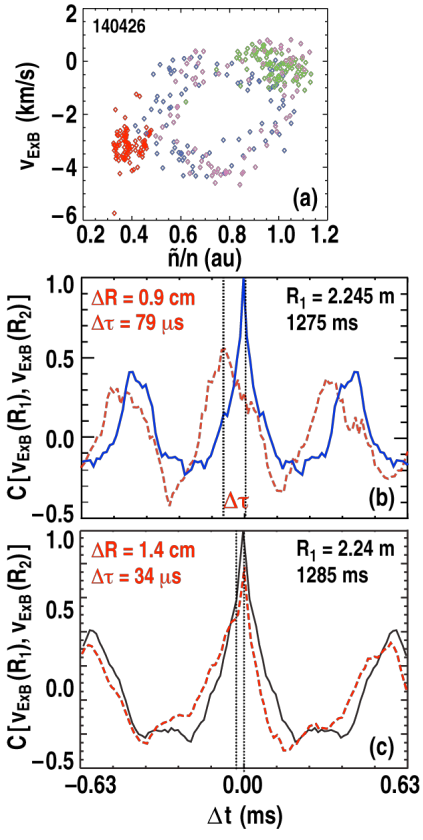

Fig. 4. (a) Limit cycle between normalized density fluctuation amplitude and **E×B** velocity; (b,c) $v_{\mathbf{E\times B}}$ autocorrelation coefficient (blue) at radius R_1 and radial cross-correlation coefficient (red) during the LCO and just before the H-mode transition.

final H-mode transition. Both of these features, as well as the diminishing LCO frequency, are consistent with the two predator/one prey model of the L-H transition [12], with Zonal Flow **E×B** shear initiating transient turbulence suppression and equilibrium shear locking in the H-mode transition.

Limit cycle oscillations were also recently observed in the H-L back-transition (Fig. 5), showing complementary behavior to the forward transition (increasing LCO/ZF frequency and decreasing $v_{E\times B}$ amplitude but similar predator-prey characteristics ($v_{E\times B}$ lags ñ by 90º), and a hysteresis in the required onset neutral beam heating power at the H-LCO transition and the LCO-L transition. Back-transition LCOs are potentially important for controlled rampdown of β_θ in ITER, as they may assist in achieving a "soft landing" of the discharge without vertical displacement events. It should be noted that the H-LCO back-transition shown in Fig. 5 is initiated by a type-I ELM event (visible in the D_α data) which may transiently reduce the equilibrium pressure gradient and related **E×B** shear. Further research is in progress to identify under what conditions back-transition LCOs can be initiated without an ELM trigger.

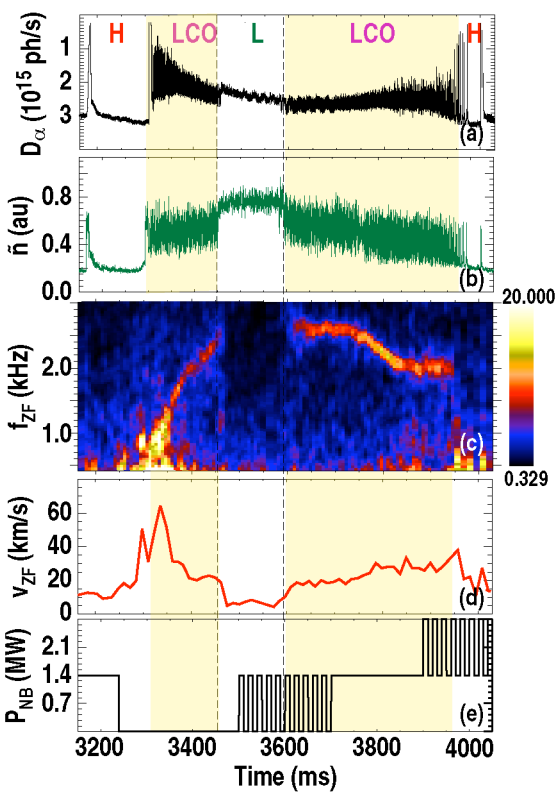

Fig. 5. (a) D_α lower divertor signal; (b) density fluctuation level; (c) limit cycle (ZF) oscillation frequency; (d) magnitude of oscillating **E×B** velocity (all measured 0.5 cm inside the LCFS); (e) neutral beam power during a sequence of H-LCO, LCO-L, L-LCO, and LCO-H transitions.

This work was supported in part by the U.S. Department of Energy under DE-FG03-01ER54615, DE-FG02-08ER54984, DE-FG02-89ER53296, DE-FG02-08ER54999 and DE-FC02-04ER54698 and DE-FG02-07ER54917.

[1] L. Schmitz, L. Zeng, T.L. Rhodes, et al., Phys. Rev. Lett. **108**, 15502-5 (2012).
[2] G. R. McKee et al., Nucl. Fusion **49**, 115016 (2009).
[3] S. J. Zweben, R. J.Maqueda,R.Hager, et al., Phys. Plasmas **17**, 102502 (2010).
[4] G. D. Conway, C. Angioni, F. Ryter, et al., Phys. Rev. Lett. **106**, 065001 (2011).
[5] G. S. Xu et al., Phys. Rev. Lett. **107**, 125001 (2011).
[6] T. Estrada, C. Hidalgo, T. Happel. et al., Phys. Rev. Lett. **107**, 245004 (2011).
[7] W.A.Peebles, T.L. Rhodes, J.C. Hillesheim, et al., Rev. Sci. Instrum. **81**, 10D902 (2010).
[8] J. C. Hillesheim et al., Rev. Sci. Instrum. **81**, 10D907 (2010).
[9] E.J. Kim and P.H. Diamond, Phys. Rev. Lett. **90**, 185006 (2003).
[10] H. Biglari, P.H. Diamond, and P.W. Terry, Phys. Fluids B **2**, 1 (1990).
[11] K.H. Burrell, Phys. Plasmas **4**, 1518 (1997).
[12] Y.H. Xu, C.X Yu, J.R. Luo et al., Phys. Rev. Lett. **18**, 3870 (2000).